Available online at www.sciencedirect.com
SCIENCE DIRECT®
Journal of Computational Physics 208 (2005) 455–468
JOURNAL OF COMPUTATIONAL PHYSICS
www.elsevier.com/locate/jcp

Efficient calculation of the steepest descent direction for source-independent seismic waveform inversion: An amplitude approach ☆

Yunseok Choi [a,*], Changsoo Shin [a], Dong-Joo Min [b], Taeyoung Ha [c]

[a] *Geophysical Prospecting Laboratory, School of Civil, Urban and Geosystem Engineering, Seoul National University, S. Korea, San 56-1, Sillim-dong, Gwanak-gu, Seoul 151-742, Korea*
[b] *Korea Ocean Research and Development Institute, S. Korea, 1270, Sa2-Dong, Sangrok-Gu, Ansan, Kyungki, 426-744, Korea*
[c] *Department of Mathematical Sciences, Seoul National University, S. Korea, San 56-1, Sillim-dong, Gwanak-gu, Seoul, 151-747, Korea*

Received 5 May 2004; received in revised form 2 September 2004; accepted 29 September 2004
Available online 11 May 2005

Abstract

In seismic waveform inversion, if we have no information on source signature, we need to invert seismic data and source signature either simultaneously or successively. In order to avoid the iterative update of the source signature in waveform inversion based on classical, local optimization techniques, we propose two source-independent objective functions using amplitude spectra of Fourier-transformed wavefields. One is constructed by normalizing the amplitude spectra of observed data and modeled data with respect to the respective reference amplitudes. The other is achieved by cross-multiplying the amplitude spectra of observed data and modeled data with the respective reference amplitudes. In the computation of the steepest descent direction, we circumvent explicitly computing the Jacobian by employing a matrix formalism of the wave equation in the frequency domain. Through numerical examples for the Marmousi model, we demonstrate that our inversion algorithms can reproduce the subsurface velocity structure without estimating source signature.

Keywords: Waveform inversion; Source-independent objective function; Steepest descent direction; Local optimization; Jacobian

☆ This work was financially supported by the National Laboratory Project of the Ministry of Science and Technology, and the Brain Korea 21 Project of the Ministry of Education.
* Corresponding author. Tel.: +82 2 875 6292; fax: +82 2 875 6296.
E-mail addresses: choi76@gpl.snu.ac.kr (Y. Choi), css@model.snu.ac.kr (C. Shin), djmin@kordi.re.kr (D.-J. Min), tyha@snu.ac.kr (T. Ha).

0021-9991/$ - see front matter © 2005 Elsevier Inc. All rights reserved.
doi:10.1016/j.jcp.2004.09.019

1. Introduction

Seismic inversion has been used to delineate the subsurface velocity structure from seismic data. Seismic inversion has been mainly performed by traveltime tomography or waveform inversion. Traveltime tomography of treating refraction or reflection events is performed on the basis of the kinematic property of seismic data [1–3], whereas waveform inversion employs the dynamic property of data [4,5]. Since traveltime tomography is a high-frequency approximation, it cannot always describe the model whose velocity variations are similar to or less than source wavelength [5]. On the other hand, waveform inversion, which is based on wave propagation, gives more refined velocity structures than traveltime tomography, although waveform inversion requires more massive computation than traveltime tomography.

In the beginning, seismic inversion was mainly performed by directly calculating the Jacobian. Since Lailly [6] and Tarantola [7] suggested using the backpropagation algorithm of reverse time migration (e.g., the adjoint state of the wave equation) in seismic inversion, the backpropagation algorithm was extensively used to elegantly compute the steepest descent direction in waveform inversion [4,8–20].

Since full waveform inversion is performed by applying wave equation, we need to know exact source signature to obtain a subsurface velocity structure that is compatible with true velocities. In the case of the exact source wavelet not being known, we iteratively estimate source wavelet in addition to velocity structure in waveform inversion algorithm. Zhou et al. [22] and Pratt [19] suggested methods of estimating source wavelet in waveform inversion algorithm, and found that the iteratively estimated source wavelet is very sensitive to estimated velocity structure. As a solution to this problem, Zhou et al. [22] suggested that successive inversions for source signature and velocity structure should be repeatedly executed until reasonable solutions for both source signature and velocity structure can be obtained. In order to avoid the additional work of inverting source wavelet, Lee and Kim [21] and Zhou and Greenhalgh [5] proposed source-independent waveform inversion algorithms, which are based on the conventional inversion technique directly computing the Jacobian. For the source-independent waveform inversion algorithm, Lee and Kim [21] used the normalized wavefields with respect to a reference wavefield in the frequency domain. The objective function constructed by Zhou and Greenhalgh [5] is similar to that by Lee and Kim [21], except that Zhou and Greenhalgh [5] only used the amplitude spectrum among spectral data obtained by the Fourier transform. Although Zhou and Greenhalgh [5] only used amplitude spectra, they obtained realistic results in the inversion of crosshole data.

In this study, we propose two different source-independent amplitude inversion algorithms. One is constructed by normalizing the amplitudes of modeled data and field data with respect to amplitudes of the respective reference wavefields like the method suggested by Zhou and Greenhalgh [5]. The other is obtained by cross-multiplying the amplitudes of modeled wavefields and field data by the respective reference amplitudes. In the former, the source wavelet is removed by deconvolution; in the latter, the source wavelet is eliminated by convolution. The main characteristic of our waveform inversion techniques is related to the computation of the steepest descent direction. In the following sections, we construct the two source-independent objective functions, and show how to compute the steepest descent direction in the source-independent waveform inversion algorithms. In order to demonstrate our waveform inversion algorithms, we present numerical examples for the Marmousi synthetic data.

2. Theory

2.1. The first source-independent objective function using deconvolution

In the frequency domain, since time series are expressed by the amplitude and phase spectra, we can write the observed data as

$$\tilde{d}_{i,j}(\omega) = A^d_{i,j} e^{i\theta^d_{i,j}}, \quad i = 1,2,\ldots,m, \;\; j = 1,2,\ldots,n, \tag{1}$$

where ω is the angular frequency, $A^d_{i,j}(\omega)$ and $\theta^d_{i,j}(\omega)$ are the amplitude and phase spectra of the observed data, respectively, and i and j denote the source and receiver points, respectively. The superscript d is used to discriminate the field data from the modeled data that will be indicated by the superscript u. If we consider ideal, 2D acoustic media without intrinsic attenuation, seismic data observed at the surface are defined as the convolution of the source wavelet and the impulse response in the time domain:

$$d_{i,j}(t) = w(t) * r_{i,j}(t), \tag{2}$$

where $w(t)$ is the source wavelet and $r_{i,j}(t)$ is the impulse response. The frequency-domain relation corresponding to Eq. (2) is given as

$$\tilde{d}_{i,j}(\omega) = \tilde{w}(\omega)\tilde{r}_{i,j}(\omega). \tag{3}$$

In Eq. (3), we note that the amplitude $A^d_{i,j}$ of Eq. (1) is composed of amplitudes of source wavelet and impulse response, as follows:

$$A^d_{i,j}(\omega) = s^d(\omega)a^d_{i,j}(\omega), \tag{4}$$

where $s^d(\omega)$ and $a^d_{i,j}(\omega)$ are the amplitudes of source wavelet and impulse response for the observed data, respectively.

If we arbitrarily choose a reference wavefield and normalize observed wavefields with respect to the reference wavefield just for amplitude spectra, we obtain

$$\frac{|\tilde{d}_{i,j}(\omega)|}{|\tilde{d}_{i,\mathrm{ref}}(\omega)|} = \frac{A^d_{i,j}(\omega)}{A^d_{i,\mathrm{ref}}(\omega)} = \frac{s^d(\omega)a^d_{i,j}(\omega)}{s^d(\omega)a^d_{i,\mathrm{ref}}(\omega)} = \frac{a^d_{i,j}(\omega)}{a^d_{i,\mathrm{ref}}(\omega)}, \tag{5}$$

where the subscript ref indicates the reference data. In Eq. (5), since source wavelet is the same, we obtain the source-independent amplitude ratio.

Similarly, we can represent the normalized amplitude of the modeled data as

$$\frac{|\tilde{u}_{i,j}(\omega)|}{|\tilde{u}_{i,\mathrm{ref}}(\omega)|} = \frac{A^u_{i,j}(\omega)}{A^u_{i,\mathrm{ref}}(\omega)} = \frac{s^u(\omega)a^u_{i,j}(\omega)}{s^u(\omega)a^u_{i,\mathrm{ref}}(\omega)} = \frac{a^u_{i,j}(\omega)}{a^u_{i,\mathrm{ref}}(\omega)}, \tag{6}$$

where the superscript u indicates the modeled data.

For source-independent waveform inversion, we define the objective function as l_2 norm of residuals between normalized amplitudes of field data and modeled data with respect to the respective reference amplitudes. The objective function is expressed for a single frequency as

$$E = \sum_i \sum_j \frac{1}{2}\left[\frac{A^u_{i,j}}{A^u_{i,\mathrm{ref}}} - \frac{A^d_{i,j}}{A^d_{i,\mathrm{ref}}}\right]^2. \tag{7}$$

The model parameter minimizing the objective function is obtained by computing the derivative of Eq. (7) with respect to the kth model parameter p_k, as follows:

$$\frac{\partial E}{\partial p_k} = \sum_i \sum_j \left(\frac{A^u_{i,j}}{A^u_{i,\mathrm{ref}}} - \frac{A^d_{i,j}}{A^d_{i,\mathrm{ref}}}\right)\frac{\partial}{\partial p_k}\left(\frac{A^u_{i,j}}{A^u_{i,\mathrm{ref}}}\right), \tag{8}$$

where the derivative of amplitude with respect to p_k is given as

$$\frac{\partial}{\partial p_k}\left(\frac{A^u_{i,j}}{A^u_{i,\mathrm{ref}}}\right)=\frac{1}{A^u_{i,\mathrm{ref}}}\left(\frac{\partial A^u_{i,j}}{\partial p_k}\right)-\frac{A^u_{i,j}}{\left(A^u_{i,\mathrm{ref}}\right)^2}\frac{\partial A^u_{i,\mathrm{ref}}}{\partial p_k}. \tag{9}$$

We can compute the partial derivative of amplitude with respect to model parameter p_k using partial derivative of the modeled wavefield with respect to p_k. The partial derivative of the modeled wavefield divided by the modeled wavefield can be written as

$$\frac{1}{\tilde{u}_{i,j}}\frac{\partial \tilde{u}_{i,j}}{\partial p_k}=\frac{1}{A^u_{i,j}}\frac{\partial A^u_{i,j}}{\partial p_k}+\mathrm{i}\frac{\partial \theta^u_{i,j}}{\partial p_k}, \tag{10}$$

and then the partial derivative of amplitude is defined as

$$\frac{\partial A^u_{i,j}}{\partial p_k}=A^u_{i,j}\,\mathrm{Re}\left\{\frac{1}{\tilde{u}_{i,j}}\frac{\partial \tilde{u}_{i,j}}{\partial p_k}\right\}. \tag{11}$$

Substituting Eqs. (9) and (11) into Eq. (8) gives

$$\frac{\partial E}{\partial p_k}=\sum_i\sum_j \mathrm{Re}\left\{\left(\frac{A^u_{i,j}}{A^u_{i,\mathrm{ref}}}-\frac{A^d_{i,j}}{A^d_{i,\mathrm{ref}}}\right)\frac{1}{A^u_{i,\mathrm{ref}}}\frac{A^u_{i,j}}{\tilde{u}_{i,j}}\frac{\partial \tilde{u}_{i,j}}{\partial p_k}-\frac{1}{A^u_{i,\mathrm{ref}}\tilde{u}_{i,\mathrm{ref}}}\frac{\partial \tilde{u}_{i,\mathrm{ref}}}{\partial p_k}\left(\frac{A^u_{i,j}}{A^u_{i,\mathrm{ref}}}-\frac{A^d_{i,j}}{A^d_{i,\mathrm{ref}}}\right)A^u_{i,j}\right\}, \tag{12}$$

which can be rewritten in a matrix form as

$$\frac{\partial E}{\partial p_k}=\sum_i \mathrm{Re}\left\{\frac{1}{A^u_{i,\mathrm{ref}}}\left[\frac{\partial \tilde{\mathbf{u}}_i}{\partial p_k}\right]^{\mathrm{T}}\begin{bmatrix}\frac{A^u_{i,1}}{\tilde{u}_{i,1}}\left(\frac{A^u_{i,1}}{A^u_{i,\mathrm{ref}}}-\frac{A^d_{i,1}}{A^d_{i,\mathrm{ref}}}\right)\\ \frac{A^u_{i,2}}{\tilde{u}_{i,2}}\left(\frac{A^u_{i,2}}{A^u_{i,\mathrm{ref}}}-\frac{A^d_{i,2}}{A^d_{i,\mathrm{ref}}}\right)\\ \vdots\\ \frac{A^u_{i,n}}{\tilde{u}_{i,n}}\left(\frac{A^u_{i,n}}{A^u_{i,\mathrm{ref}}}-\frac{A^d_{i,n}}{A^d_{i,\mathrm{ref}}}\right)\end{bmatrix}-\frac{C_{i,\mathrm{ref}}}{A^u_{i,\mathrm{ref}}}\left[\frac{\partial \tilde{\mathbf{u}}_i}{\partial p_k}\right]^{\mathrm{T}}\begin{bmatrix}0\\ \vdots\\ \frac{1}{\tilde{u}_{i,\mathrm{ref}}}\\ 0\\ \vdots\end{bmatrix}\right\} \tag{13}$$

with

$$C_{i,\mathrm{ref}}=\sum_j\left[\left(\frac{A^u_{i,j}}{A^u_{i,\mathrm{ref}}}-\frac{A^d_{i,j}}{A^d_{i,\mathrm{ref}}}\right)A^u_{i,j}\right]. \tag{14}$$

We can rewrite the gradient vector as

$$\frac{\partial E}{\partial p_k}=\sum_i \mathrm{Re}\left\{\frac{1}{A^u_{i,\mathrm{ref}}}\left[\frac{\partial \tilde{\mathbf{u}}_i}{\partial p_k}\right]^{\mathrm{T}}\mathbf{r}_i\right\}, \tag{15}$$

where $\mathbf{r}_i$ is the residual vector whose components are expressed as

$$r_{i,j}=\begin{cases}\frac{A^u_{i,j}}{\tilde{u}_{i,j}}\left(\frac{A^u_{i,j}}{A^u_{i,\mathrm{ref}}}-\frac{A^d_{i,j}}{A^d_{i,\mathrm{ref}}}\right), & j\neq \mathrm{ref},\\ \frac{A^u_{i,j}}{\tilde{u}_{i,j}}\left(\frac{A^u_{i,j}}{A^u_{i,\mathrm{ref}}}-\frac{A^d_{i,j}}{A^d_{i,\mathrm{ref}}}\right)-\frac{C_{i,\mathrm{ref}}}{\tilde{u}_{i,\mathrm{ref}}}, & j=\mathrm{ref}.\end{cases} \tag{16}$$

In Eqs. (15) and (16), if we compute the partial derivative wavefield for an entire model parameter and augment the residual vector by adding zeroes, we can express the total gradient for the entire model parameter as

$$\frac{\partial E}{\partial \mathbf{p}} = \sum_i \mathrm{Re}\left\{ \frac{1}{A^u_{i,\mathrm{ref}}} \left[\frac{\partial \tilde{\mathbf{u}}_i}{\partial \mathbf{p}} \right]^{\mathrm{T}} \mathbf{r}_i \right\} \tag{17}$$

with

$$r_{i,k} = \begin{cases} \frac{A^u_{i,k}}{\tilde{u}_{i,k}} \left(\frac{A^u_{i,k}}{A^u_{i,\mathrm{ref}}} - \frac{A^d_{i,k}}{A^d_{i,\mathrm{ref}}} \right), & k = j \text{ and } k \neq \mathrm{ref}, \\ \frac{A^u_{i,k}}{\tilde{u}_{i,k}} \left(\frac{A^u_{i,k}}{A^u_{i,\mathrm{ref}}} - \frac{A^d_{i,k}}{A^d_{i,\mathrm{ref}}} \right) - \frac{C_{i,\mathrm{ref}}}{\tilde{u}_{i,\mathrm{ref}}}, & k = j \text{ and } k = \mathrm{ref}, \\ 0, & k \neq j, \end{cases} \tag{18}$$

where j indicates the receiver point.

In Eq. (17), the partial derivatives of the modeled wavefields can be expressed by using the forward modeling operator $\mathbf{S}$ and the virtual source matrix $\mathbf{V}$, as they are in the reverse-time migration (e.g., Eqs. (A.8)–(A.12) in Appendix A) [26], which results in

$$\frac{\partial E}{\partial \mathbf{p}} = \sum_i \sum_\omega \mathrm{Re}\left\{ \frac{1}{A^u_{i,\mathrm{ref}}} \mathbf{V}_i^{\mathrm{T}} [\mathbf{S}^{-1}]^{\mathrm{T}} \mathbf{r}_i \right\} \Delta\omega \tag{19}$$

for the entire frequency. By comparing Eq. (19) with Eq. (A.11) for the reverse-time migration, we can note that the source-independent waveform inversion has the same numerical algorithm as that of the reverse-time migration. In Eq. (19), since the forward modeling operator $\mathbf{S}$ is symmetric and the self adjoint, the term $[\mathbf{S}^{-1}]^{\mathrm{T}}\mathbf{r}_i$ implies backpropagating the residuals. As a result, we can determine the steepest descent direction by backpropagating the residuals between normalized amplitudes of observed data and modeled data, and then convolving the backpropagated residuals with the virtual source (e.g., Appendix A; [26]).

In this source-independent waveform inversion, we note that the reference wavefields can be arbitrarily chosen among wavefields observed or computed at all the receiver points. As an alternative of the inversion, we can also repeat the inversion process one by one so that wavefields of all the receivers can be the reference wavefield, and then average the resulting velocity models.

2.2. Source-independent objective function using convolution

An alternative to building a source-independent objective function is to cross-multiply both observed data and modeled data by the respective reference amplitudes. In this case, the objective function can be given at a single frequency as

$$\begin{aligned} E &= \sum_i \sum_j \frac{1}{2} \left[A^d_{i,\mathrm{ref}}(\omega) A^u_{i,j}(\omega) - A^u_{i,\mathrm{ref}}(\omega) A^d_{i,j}(\omega) \right]^2 \\ &= \sum_i \sum_j \frac{1}{2} \left[a^d_{i,\mathrm{ref}}(\omega) s^d(\omega) a^u_{i,j}(\omega) s^u(\omega) - a^u_{i,\mathrm{ref}}(\omega) s^u(\omega) a^d_{i,j}(\omega) s^d(\omega) \right]^2. \end{aligned} \tag{20}$$

Since the amplitudes of source wavelets for both observed data and modeled data are included in both terms, the source effect also disappears in this objective function. Similarly to the former source-independent waveform inversion using deconvolution, we can compute the steepest descent direction for the entire frequency by using

$$\frac{\partial E}{\partial \mathbf{p}} = \sum_i \sum_\omega \mathrm{Re}\left\{ \mathbf{V}_i^{\mathrm{T}} [\mathbf{S}^{-1}]^{\mathrm{T}} \mathbf{r}_i \right\} \Delta\omega \tag{21}$$

with the residual vector

$$r_{i,k} = \begin{cases} \frac{A^d_{i,\mathrm{ref}} A^u_{i,k}}{\tilde{u}_{i,k}} \left(A^d_{i,\mathrm{ref}} A^u_{i,k} - A^u_{i,\mathrm{ref}} A^d_{i,k} \right), & k = j \text{ and } k \neq \mathrm{ref}, \\ \frac{A^d_{i,\mathrm{ref}} A^u_{i,k}}{\tilde{u}_{i,k}} \left(A^d_{i,\mathrm{ref}} A^u_{i,k} - A^u_{i,\mathrm{ref}} A^d_{i,k} \right) - \frac{C'_{i,\mathrm{ref}}}{\tilde{u}_{i,\mathrm{ref}}}, & k = j \text{ and } k = \mathrm{ref}, \\ 0, & k \neq j, \end{cases} \tag{22}$$

where

$$C'_{i,\mathrm{ref}} = \sum_j A^u_{i,\mathrm{ref}} A^d_{i,j} \left[A^d_{i,\mathrm{ref}} A^u_{i,j} - A^u_{i,\mathrm{ref}} A^d_{i,j} \right]. \tag{23}$$

In this source-independent objective function using convolution, we also propagate the residuals of weighted amplitudes, and then compute the gradient vector by calculating the zero-lag value of convolution between the backpropagated residual and the virtual source.

3. Numerical examples

We test our source-independent waveform inversion algorithms for synthetic data of the IFP Marmousi model [23]. Fig. 1 shows the Marmousi model with the grid interval of 16 m. In Fig. 1, horizontal and vertical distances of the Marmousi model are 9.2 and 3 km, respectively. We generate synthetic seismograms of the Marmousi model using the 9-point frequency-domain finite-difference operator suggested by Jo et al. [24] for 61 frequencies ranging from 0.3 to 18.75 Hz. We locate 556 shots with intervals of 16 m at the surface: The first shot lies at 0.16 km, and the last shot is located at 9.04 km. For each shot, we place 576 receivers at all the surface nodal points. Fig. 2 shows an example of synthetic seismogram generated for the Marmousi model, when a source is located at the distance of 4.016 km.

For an initial model of waveform inversion, we choose a linearly increasing velocity structure whose velocity varies from 1.5 to 4.5 km/s with depth as shown in Fig. 3(a). Fig. 3(b) shows the velocity model inverted by the first source-independent waveform inversion algorithm using normalized amplitudes at the 100th iteration, whereas Fig. 3(c) shows the finally inverted velocity model at the 360th iteration. In Fig. 3(c), the velocity of the shallow subsurface is compatible with the true velocity model. Although the

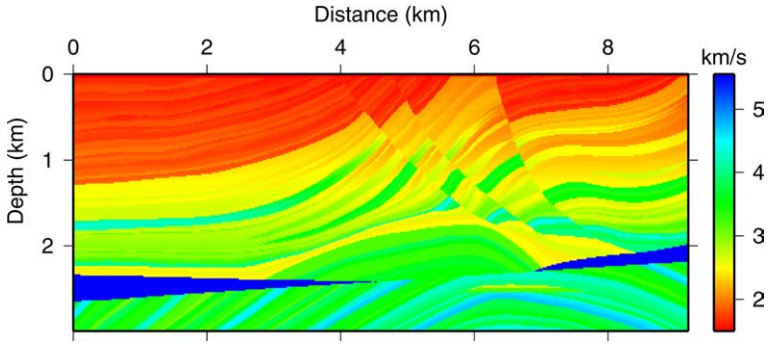

Fig. 1. The Marmousi model with the grid interval of 16 m.

deeper subsurface also converges with the true velocity model as the iteration increases, the reservoir and its neighboring structure are not clearly seen in the finally inverted velocity model. Furthermore, the left and the right part of the inverted velocity structure are still far from the true velocity structure. Fig. 4 shows the history of rms error. The rms error slowly decreases as the inverted velocity approximates the true velocity model.

Fig. 5(a) and (b) shows the velocity models inverted by the second source-independent inversion algorithm using convolution at the 100th and 360th iterations, respectively. From Fig. 5(b), we note that the inverted velocity model is almost the same as that of the first objective function using normalized amplitude (e.g., Fig. 3(c)). Fig. 6 shows the history of rms error, which is also similar to that of the first objective function.

In general, since low-frequency components of real data are mixed with noise, we often discard low-frequency components less than 5 Hz in seismic data processing. In order to investigate if our algorithm can be applied to data that are lacking low-frequency components, we also test the first inversion algorithm using deconvolution for the Marmousi synthetic data without frequencies less than 5 Hz. Fig. 7 shows the inverted velocity model at the 250th iteration. By comparing Fig. 7 to Fig. 3(c), we note that although shallow subsurface structure is comparable to the true velocity model, the resolution of the

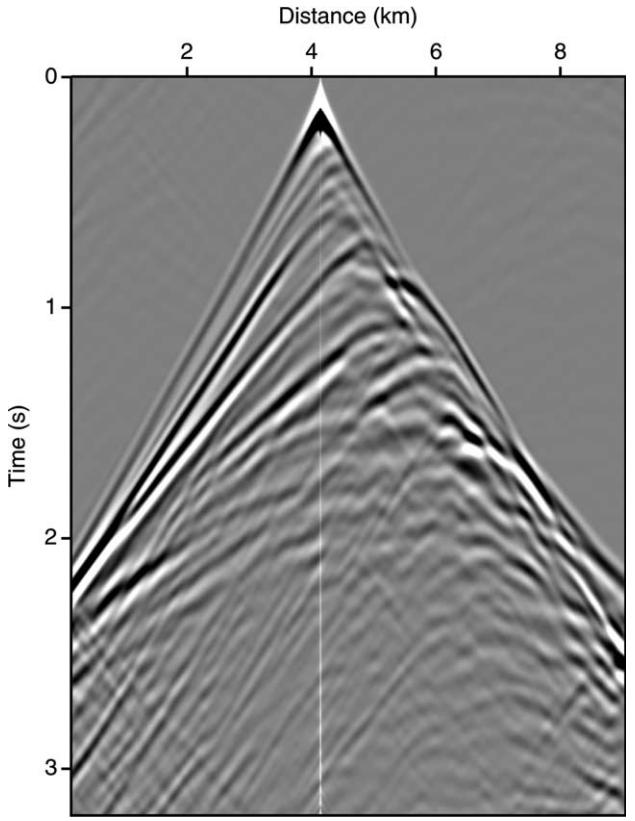

Fig. 2. A synthetic seismogram generated by using 9-point frequency-domain finite-difference operator for the Marmousi model, when a source is located at 4.016 km.

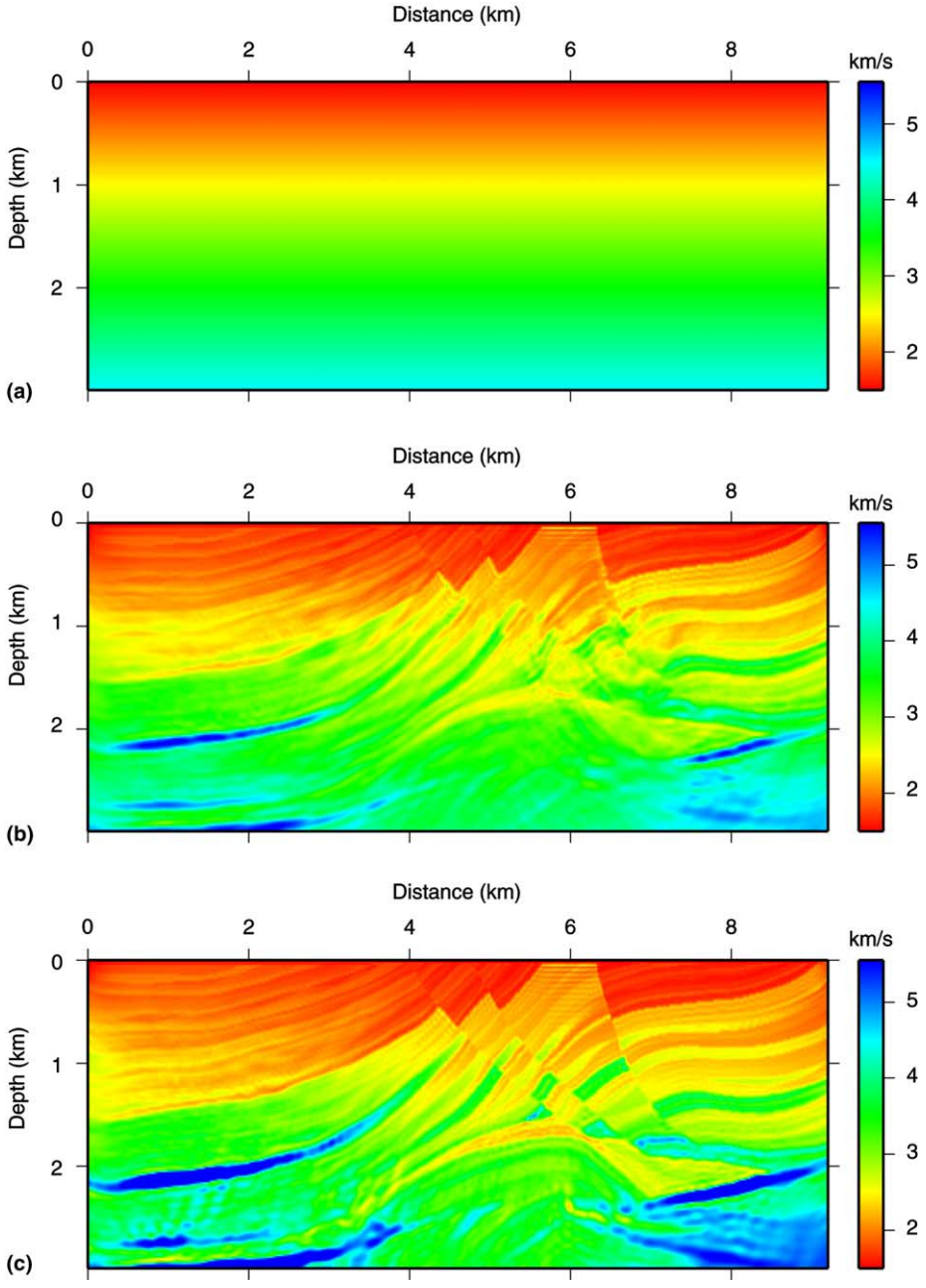

Fig. 3. Numerical examples of the first source-independent waveform inversion using deconvolution for the Marmousi model: (a) initial velocity model, (b) the 100th inverted velocity model and (c) the 360th inverted velocity model.

whole structure is not as good as that obtained by using the entire frequency band. Fig. 8 shows the history of rms error. In Fig. 8 we see that the rms error decreases to 10% of initial value, which is larger than that of entire frequency data.

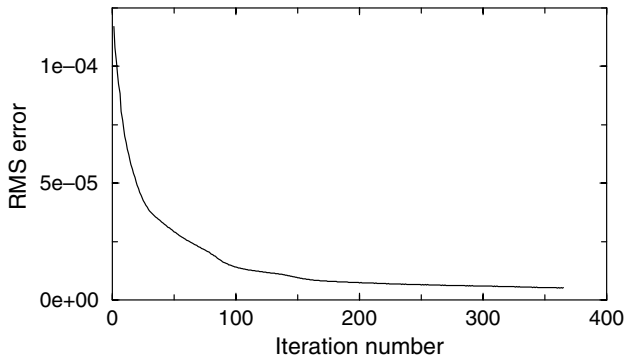

Fig. 4. The history of rms error in the first source-independent waveform inversion using deconvolution.

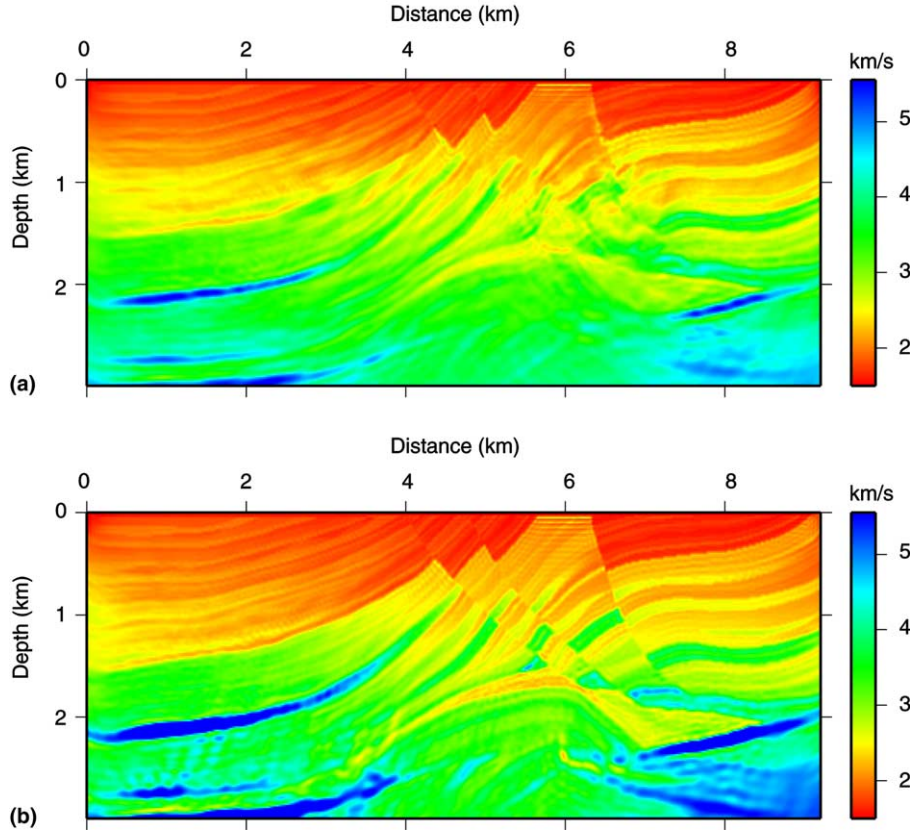

Fig. 5. Numerical examples of the second, source-independent waveform inversion using convolution for the Marmousi model: (a) the 100th and (b) 360th inverted velocity models.

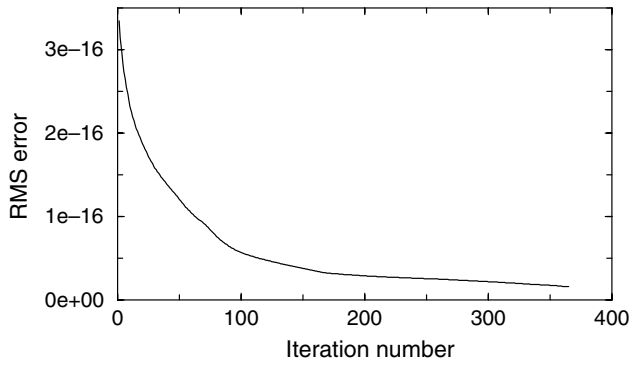

Fig. 6. The history of rms error in the second, source-independent waveform inversion using convolution.

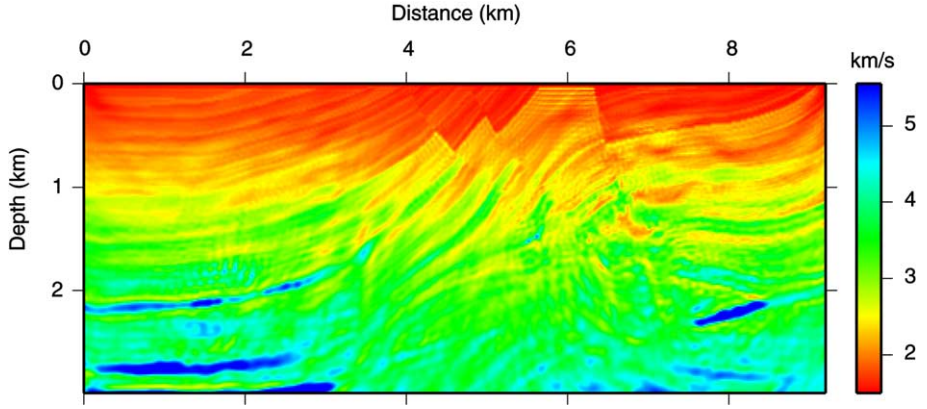

Fig. 7. The velocity model inverted by the first, source-independent waveform inversion for the Marmousi synthetic data without low-frequency information less than 5 Hz at the 250th iteration.

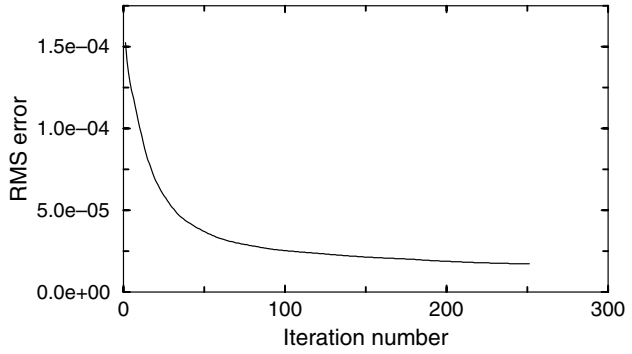

Fig. 8. The history of rms error in the first, source-independent waveform inversion for the Marmousi synthetic data without low-frequency information less than 5 Hz.

4. Conclusion

We presented two source-independent seismic inversion algorithms employing amplitude spectra of Fourier-transformed wavefields. In our algorithms, we constructed source-independent objective functions by either deconvolution (expressed by dividing in the frequency domain) or convolution (described by multiplying in the frequency domain). In the case of deconvolution, we normalized amplitudes of modeled data and observed data with respect to the respective reference amplitudes and then defined the objective function as the l_2 norm between residuals of the normalized amplitudes. On the other hand, in the case of convolution, we cross-multiplied amplitudes of modeled data and observed data with the respective reference amplitudes. The reference wavefield can be arbitrarily chosen among wavefields at surface receiver points. For the calculation of the steepest descent direction, we did not directly compute the Jacobian, but used the backpropagation technique of reverse time migration on the basis of the symmetry of Green's function. The numerical algorithm of our inversion techniques is equivalent to that of conventional pre-stack reverse time migration and waveform inversion.

From numerical examples for the Marmousi synthetic data, we note that our inversion algorithm gives inverted velocity structures compatible with true velocity models without numerically estimating source signature. In order to demonstrate the feasibility of our algorithm to real data, we also tested our algorithms for the Marmousi synthetic data without low frequencies less than 5 Hz. In this case, although the velocity model inverted without low frequencies is not as good as that of whole frequency data, the inverted velocity structure is still comparable to the true velocity structure. In spite of these numerical examples, we still hesitate to assert that our source-independent waveform inversion algorithms can be applied to real data collected in the 3D elastic media causing mode conversion, scattering, and intrinsic attenuation, because we construct our algorithms on the assumption of the ideal, 2D acoustic media. Application of our algorithms to real data may require some correction for 3D elastic effects, a topic that will be studied in the future.

Considering that the waveform inversion employs the same numerical algorithm as reverse time migration, we expect that our source-independent algorithm can be applied to the reverse-time migration without estimating the source wavelet. In the future, we will apply our source-independent algorithm to 2D elastic, 3D acoustic, and 3D elastic waveform inversions. We can also extend our algorithm to time-domain waveform inversions.

Appendix A. Reverse time migration

We examine numerical algorithm of 2D reverse-time migration following the 1D reverse-time migration algorithm presented by Shin et al. [26]. Since the partial derivative wavefield with respect to the model parameter can be interpreted as the sensitivity of wavefields to the perturbation of model parameter [27], we can establish a numerical expression of the migrated image for the kth model parameter, as follows:

$$\phi_k = \sum_i \sum_j \sum_t \frac{\partial u_{i,j}(t)}{\partial p_k} d_{i,j}(t), \quad i = 1, 2, \ldots, N_s, \text{ and } j = 1, 2, \ldots, N_r, \tag{A.1}$$

where $u_{i,j}$ and $d_{i,j}$ are the modeled data and the observed data, respectively, and i and j indicate the source and receiver points, respectively.

In the frequency domain, the equivalent of Eq. (A.1) can be written as

$$\phi_k = \sum_i \sum_j \sum_\omega \frac{\partial \tilde{u}_{i,j}(\omega)}{\partial p_k} \tilde{d}^*_{i,j}(\omega) \tag{A.2}$$

or

$$\phi_k = \sum_i \sum_j \sum_\omega \frac{\partial \tilde{u}^*_{i,j}(\omega)}{\partial p_k} \tilde{d}_{i,j}(\omega), \tag{A.3}$$

where $\tilde{d}_{i,j}(\omega)$ and $[\partial \tilde{u}_{i,j}(\omega)/\partial p_k]$ are the Fourier transforms of $d_{i,j}(t)$ and $[\partial u_{i,j}(t)/\partial p_k]$, respectively, and * denotes the complex conjugate. For convenience, we consider a single frequency, which allows us to omit the summation about frequency.

In Eq. (A.2), the migrated image is described by the field data observed at the surface receiver points and the partial derivative wavefields computed at the surface receiver points. We can rewrite Eq. (A.2) by using the partial derivative wavefield for an entire model parameter, as follows:

$$\mathbf{\Phi} = \sum_i \begin{bmatrix} \frac{\partial \tilde{u}_{i,1}(\omega)}{\partial p_1} & \cdots & \frac{\partial \tilde{u}_{i,N_r}(\omega)}{\partial p_1} & \frac{\partial \tilde{u}_{i,N_{r+1}}(\omega)}{\partial p_1} & \cdots & \frac{\partial \tilde{u}_{i,K}(\omega)}{\partial p_1} \\ \frac{\partial \tilde{u}_{i,1}(\omega)}{\partial p_2} & \cdots & \frac{\partial \tilde{u}_{i,N_r}(\omega)}{\partial p_2} & \frac{\partial \tilde{u}_{i,N_{r+1}}(\omega)}{\partial p_2} & \cdots & \frac{\partial \tilde{u}_{i,K}(\omega)}{\partial p_2} \\ \vdots & & \vdots & \vdots & \ddots & \vdots \\ \frac{\partial \tilde{u}_{i,1}(\omega)}{\partial p_K} & \cdots & \frac{\partial \tilde{u}_{i,N_r}(\omega)}{\partial p_K} & \frac{\partial \tilde{u}_{i,N_{r+1}}(\omega)}{\partial p_K} & \cdots & \frac{\partial \tilde{u}_{i,K}(\omega)}{\partial p_K} \end{bmatrix} \begin{bmatrix} \tilde{d}^*_{i,1}(\omega) \\ \vdots \\ \tilde{d}^*_{i,N_r}(\omega) \\ 0 \\ \vdots \\ 0 \end{bmatrix}. \tag{A.4}$$

Eq. (A.4) can be expressed in a matrix form as

$$\mathbf{\Phi} = \sum_i \left[\frac{\partial \tilde{\mathbf{u}}_i(\omega)}{\partial \mathbf{p}}\right]^{\mathrm{T}} \mathbf{r}^*_i(\omega) \tag{A.5}$$

with

$$r_{i,k}(\omega) = \begin{cases} \tilde{d}_{i,k}(\omega), & k = j, \\ 0, & k \neq j, \end{cases} \tag{A.6}$$

where j indicates the surface receiver point.

In a similar method, Eq. (A.3) can be expressed as

$$\mathbf{\Phi} = \sum_i \left[\frac{\partial \tilde{\mathbf{u}}^*_i(\omega)}{\partial \mathbf{p}}\right]^{\mathrm{T}} \mathbf{r}_i(\omega). \tag{A.7}$$

The partial derivative wavefields in Eqs. (A.5) and (A.7) can be computed by taking the derivative of the matrix equation given in forward modeling.

In forward modeling of wave equation using frequency-domain finite-difference or finite-element methods, we solve the discretized matrix equation written for a single frequency by

$$\mathbf{S}(\omega)\tilde{\mathbf{u}}_i(\omega) = \mathbf{f}_i(\omega), \tag{A.8}$$

where $\mathbf{S}(\omega)$ is the complex impedance matrix and $f_i(\omega)$ is the ith source vector [25]. Taking the partial derivative of Eq. (A.8) with respect to the kth model parameter p_k gives

$$\mathbf{S}(\omega)\frac{\partial \tilde{\mathbf{u}}_i(\omega)}{\partial p_k} = -\frac{\partial \mathbf{S}(\omega)}{\partial p_k}\tilde{\mathbf{u}}_i(\omega) \quad \text{or} \quad \frac{\partial \tilde{\mathbf{u}}_i(\omega)}{\partial p_k} = \mathbf{S}^{-1}(\omega)\mathbf{v}_{i,k}(\omega) \tag{A.9}$$

with

$$\mathbf{v}_{i,k}(\omega) = -\frac{\partial \mathbf{S}(\omega)}{\partial p_k}\tilde{\mathbf{u}}_i(\omega), \tag{A.10}$$

where $\mathbf{v}_{i,k}(\omega)$ is defined as the virtual source vector with respect to the kth model parameter [4].

On the basis of Eqs. (A.9) and (A.10), we can rewrite Eqs. (A.5) and (A.7) for an entire frequency band as

$$\mathbf{\Phi} = \sum_i \sum_\omega \mathbf{V}_i^{\mathrm{T}}(\omega)[\mathbf{S}^{-1}(\omega)]^{\mathrm{T}}\mathbf{r}_i^*(\omega) \tag{A.11}$$

or

$$\mathbf{\Phi} = \sum_i \sum_\omega \mathbf{V}_i^{*\mathrm{T}}(\omega)[\mathbf{S}^{-1}(\omega)]^{*\mathrm{T}}\mathbf{r}_i(\omega), \tag{A.12}$$

where $\mathbf{V}_i(\omega)$ is the ith virtual source matrix, whose column is the virtual source vector $\mathbf{v}_{i,k}(\omega)$ with respect to the kth model parameter:

$$\mathbf{V}_i(\omega) = [\mathbf{v}_{i,1}(\omega)\mathbf{v}_{i,2}(\omega)\cdots\mathbf{v}_{i,N}(\omega)]. \tag{A.13}$$

Note that the complex conjugate in the frequency domain represents time-reverse in the time domain, and the forward modeling operator $\mathbf{S}$ is symmetric. Then, the product of the last two terms $[\mathbf{S}^{-1}(\omega)]^{\mathrm{T}}\mathbf{r}_i^*(\omega)$ in Eq. (A.11) describes downward-propagation of the time-reverse surface wavefield. In Eq. (A.11), we can obtain a migrated image by downward propagating time-reversed surface wavefields and then convolving the downward-propagated wavefields with the virtual source. Similarly, in Eq. (A.12), a migrated image is obtained by backpropagating normal (unreversed) surface wavefields and then taking the zero-lag cross-correlation between the backpropagated wavefields and the virtual source. Eq. (A.12) is a general frequency-domain expression of reverse-time migration that is mainly implemented by time-reversed marching of surface data in the time domain. In the frequency domain, however, we favor Eq. (A.11), which is an alternative expression of reverse-time migration.

References

[1] G. Nolet, Seismic Wave Propagation and Seismic Tomography with Applications in Global Seismology and Exploration Geophysics, Reidel, Dordrecht, 1987.
[2] N.D. Bregman, R.C. Bailey, C.H. Chapman, Crosshole seismic tomography, Geophysics 54 (1989) 200–215.
[3] Y. Luo, G.T. Schuster, Wave-equation traveltime inversion, Geophysics 56 (1991) 645–653.
[4] R.G. Pratt, C.S. Shin, G.J. Hicks, Gauss–Newton and full Newton methods in frequency-space seismic waveform inversion, Geophys. J. Int. 133 (1998) 341–362.
[5] B. Zhou, S.A. Greenhalgh, Crosshole seismic inversion with normalized full-waveform amplitude data, Geophysics 68 (2003) 1320–1330.
[6] P. Lailly, The seismic inverse problem as a sequence of before stack migration, in: J.B. Bednar, R. Redner, E. Robinson, A. Weglein (Eds.), Conference on Inverse Scattering: Theory and Application, Soc. Industr. Appl. Math (1983).
[7] A. Tarantola, Inversion of seismic reflection data in the acoustic approximation, Geophysics 49 (1984) 1259–1266.
[8] A. Bamberger, G. Chavent, C. Hemon, P. Lailly, Inversion of normal incidence seismograms, Geophysics 46 (1982) 757–770.
[9] P. Kolb, F. Collino, P. Lailly, Prestack inversion of a 1-D mdium, Proc. IEEE 74 (1986) 498–506.
[10] O. Gauthier, J. Vriieux, A. Tarantola, Two-dimensional nonlinear inversion of seismic waveforms: numerical results, Geophysics 51 (1986) 1387–1403.
[11] A. Trantola, A strategy for nonlinear elastic inversion of seismic reflection data, Geophysics 51 (1986) 1893–1903.
[12] A. Trantola, G. Jobert, D. Trezeguet, E. Denelle, The nonlinear inversion of seismic waveforms can be performed either time extrapolation or by depth extrapolation, Geophys. Prospect. 36 (1988) 383–416.
[13] P. Mora, Nonlinear two-dimensional elastic inversion of multioffset seismic data, Geophysics 52 (1987) 1211–1228.
[14] R. Sun, G.A. McMechan, Full-wavefield inversion of wide-aperture SH and Love wave data, Geophys. J. Int. 111 (1992) 1–10.
[15] D. Cao, W.B. Beydoun, S.C. Singh, A. Trantola, A simultaneous inversion for background velocity and impedance maps, Geophysics 55 (1990) 458–469.
[16] A. Pica, J.P. Diet, A. Tarantola, Nonlinear inversion of seismic reflection data in a laterally invariant medium, Geophysics 55 (1990) 284–292.
[17] T. Xu, G.A. McMechan, R. Sun, 3-D pretack full-wavefield inversion, Geophysics 60 (1995) 1805–1818.

[18] C. Zhou, W. Cai, Y. Luo, G.T. Schuster, S. Hassanzadeh, Acoustic wave equation traveltime and waveform inversion of cross hole seismic data, Geophysics 60 (1995) 765–773.
[19] R.G. Pratt, Seismic waveform inversion in the frequency domain, Part 1: Theory and verification in a physical scale model, Geophysics 64 (1999) 888–901.
[20] R.G. Pratt, R.M. Shipp, Seismic waveform inversion in the frequency domain, Part 2: Falt delineation in sediments using crosshole data, Geophysics 64 (1999) 902–914.
[21] K.H. Lee, H.J. Kim, Source-independent full-waveform inversion of seismic data, Geophysics 68 (2003) 2010–2015.
[22] C. Zhou, G.T. Schuster, S. Hassanzadeh, J.M. Harris, Elastic wave equation traveltime and waveform inversion of crosswell data, Geophysics 62 (1997) 853–869.
[23] R. Versteeg, The Marmousi experience: Velocity model determination on a synthetic complex data set, The Leading Edge 13 (1994) 927–936.
[24] C.H. Jo, C.S. Shin, J.H. Suh, Design of an optimal 9 point finite difference frequency-space acoustic wave equation scheme for inversion and modeling, Geophysics 61 (1996) 329–337.
[25] K.J. Marfurt, Accuracy of finite-difference and finite-element modeling of the scalar and elastic wave-equations, Geophysics 49 (1984) 533–549.
[26] C. Shin, D.-J. Min, D. Yang, S.K. Lee, Evaluation of poststack migration in terms of virtual source and partial derivative wavefields, J. Seism. Explor. 12 (2003) 17–37.
[27] C. Shin, S. Chung, Understanding CMP stacking hyperbola in terms of partial derivative wavefield, Geophysics 64 (1999) 1774–1782.